AAS 25-352

JAMES WEBB SPACE TELESCOPE FUEL SLOSH ESTIMATION

Thi-han W. Nge[*], Matthew M. Wittal[†], Carl Hansen[‡], and Peter Gauthier[§]

The mitigation of fuel slosh in microgravity environments is a pressing matter for the control of both manned and unmanned spacecraft. Recent work has investigated negative mass modeling of fuel slosh using Lie Group $\mathsf{SE}(3)$. This paper applies Lie group $\mathsf{SE}(3)$ to the full body problem of spacecraft dynamics to investigate attitude perturbations caused by fuel slosh aboard the James Webb Space Telescope (JWST). We develop a dynamical model to parse these perturbations from slew telemetry data via residuals analysis. This model uses a novel, N-body Runge-Kutta integrator in the special Euclidean group $\mathsf{SE}(3)$. Frequency analysis of the resulting angular velocity residuals did not yield the expected slosh modes.

INTRODUCTION

NASA's Artemis Program to return humans to the Moon will require spacecraft to perform rendezvous, proximity operations, and docking (RPOD) while carrying unprecedented quantities of fuel [1, 2]. Fuel slosh can negatively impact spacecraft stability, and has been a topic of interest for the past several decades. For example, [3] has recently shown that both spacecraft angular velocity and fuel fill level can affect spacecraft stability. The equivalent mechanical models used in [3] had been developed as early as 1967 in [4]. These variable slosh dynamics enable a large range slosh mode frequencies, damping ratios, and slosh forces throughout the operational life of a spacecraft [5]. As such, fuel slosh can present a major complication to the guidance, navigation, and control (GN&C) of spacecraft [6]. [7] outlines the strong coupling between spacecraft rigid-body dynamics and fuel motion that almost derailed Apollo missions 8, 10, and 11.

An important application of fuel slosh mitigation is that of space telescopes, which have extremely high precision requirements for pointing stability [8]. The infrared-observing James Webb Space Telescope (JWST), launched on December 25, 2021, requires a coarse pointing stability of > 1 arcsecond deviation over 0.1 seconds [9]. Only then can fine guidance and data acquisition begin. The JWST carries up to 301 kg of hypergolic propellants to maintain its unstable orbit around the Sun-Earth Lagrange 2 (L2) point [10, 11]. This represents up to 5% of the JWST's total mass.

Simpler mathematical models for fuel slosh, such as the spring-mass-damper or pendulum methods, are poor approximations of complex tank geometries and sloshing in the microgravity do-

[*]Recent Graduate, Department of Ocean and Mechanical Engineering, Florida Atlantic University, 777 Glades Rd, Boca Raton, FL 33431

[†]Automation and Robotics Systems Engineer, Granular Mechanics and Regolith Operations Laboratory, NASA Kennedy Space Center, FL 32899, and Ph.D. Candidate, Embry-Riddle Aeronautical University, 1 Aerospace Blvd., Daytona Beach, FL 32114

[‡]JWST Spacecraft Systems Engineer, SEITO Flight Systems Engineering Branch, Space Telescope Science Institute, 3700 San Martin Drive, Baltimore, MD 21218

[§]JWST Principal Flight Systems Engineer, Flight Systems Engineering Branch, Space Telescope Science Institute, 3700 San Martin Drive, Baltimore, MD 21218

main [12, 13]. Propellant management devices (PMDs) are one such example of a complex tank geometry and one that is used by the JWST [14]. Accordingly, more accurate models can be computationally intensive and as of the time of writing none have been successfully validated by on-orbit data. In reviewing the state of the art, [15] identified the lack of low-g slosh model validation including the accurate measurement of vehicle motion, liquid motion, and initial conditions/disturbance inputs. The SPHERES Slosh Experiment aboard International Space Station (ISS), further discussed in [16], specifically struggled to accurately measure vehicle motion. Logistical and operational constraints, such as the budgeting of spacecraft time, propellant budget, and upmass, can often hinder validation efforts. The analysis of slew telemetry data for the purpose of fuel slosh estimation offers the validation of fuel slosh models without interruption to the spacecraft's science mission.

In this paper, an algorithm is developed to perform fuel slosh estimation for JWST using on-orbit slew telemetry data provided by the Space Telescope Science Institute (STScI). Instead of modeling the fluid as in [17], this paper opts to model the spacecraft dynamics. An N-body, 6-DoF dynamical model is developed to simulate the attitude perturbations expected for the JWST in orbit without the effects of fuel slosh. This simulated attitude data may then be used for residuals analysis to identify fuel slosh behavior and other low frequency vibrations. The accurate identification of JWST fuel slosh frequency and damping ratio could allow for the future implementation of control algorithms, such as input shaping, to minimize slosh excitation during slews [18–20]. [21] specifies that this accurate identification of slosh behavior can directly contribute to the design of a faster-acting input shaper that more effectively suppresses target frequencies. The formulation of this dynamical model on Lie group $\mathsf{SE}(3)$ enables the consideration of orbit-attitude coupling without the singularities, unwinding, or nonuniqueness issues present in other attitude parameterization sets [22, 23].

PRELIMINARIES

The phase space of a system refers to all possible combinations of an object's position and momentum. For a rigid body in Euclidean 3-space $\mathbb{R}^3$, this phase space contains twelve dimensions–six for translation and six for rotation.

Attitude information is typically parameterized using principal rotation angles, Euler angles, Rodrigues parameters, or quaternions [24]. This paper instead looks to Lie groups for their use of rotation matrices. Group theory refers to subsets of the phase space that are related by the four group theory axioms: closure, associativity, identity, and invertibility [25]. The special orthogonal group $\mathsf{SO}(3)$, also known as the 3D rotation group, is the subset of a system's phase space that denotes rotations in $\mathbb{R}^3$. This special behavior is because all special orthogonal matrices have a determinant of 1, unlike matrices in the orthogonal group $\mathsf{O}(3)$. Of particular interest in this paper is the special Euclidean group $\mathsf{SE}(3)$. $\mathsf{SE}(3)$ is a subset of a system's phase space that denotes all 3D transformations (both translations and rotations) in $\mathbb{R}^3$. It uses a rotation matrix $R \in \mathsf{SO}(3)$. Both $\mathsf{SO}(3)$ and $\mathsf{SE}(3)$ are considered Lie groups.

Formulation on Special Euclidean Group $\mathsf{SE}(3)$

The pose of a rigid body is expressed in $\mathsf{SE}(3)$ as

$$g = \begin{bmatrix} R & r \\ 0_{1\times 3} & 1 \end{bmatrix} \in \mathsf{SE}(3) \tag{1}$$

where $R \in \mathsf{SO}(3)$ is the rotation matrix from the body frame $\mathcal{B}$ to the inertial frame $\mathcal{N}$ and r is the position vector in the inertial frame. The smoothness of the matrix Lie group implies the existence of a single tangent space at each point. The tangent space at the identity element of the group is referred to as Lie algebra [26] and is denoted as

$$\mathfrak{se}(3) = \left\{ V^\vee = \begin{bmatrix} \omega^\times & v \\ 0_{1\times 3} & 0 \end{bmatrix},\ \omega^\times \in \mathfrak{so}(3),\ v \in \mathbb{R}^3 \right\} \tag{2}$$

where $(\cdot)^\vee$ indicates the wedge map, i.e. $(\cdot)^\vee : \mathbb{R}^6 \to \mathfrak{se}(3)$ applied to the vector $\mathbb{V} = [\omega^T,\, v^T]^T$ which is the augmented velocity vector, defined through the translational velocity $v \in \mathbb{R}^3$ and the angular velocity $\omega \in \mathbb{R}^3$; $\mathfrak{so}(3)$ is the set of 3 by 3 skew symmetric matrices such that $\omega^\times$ can be defined in terms of the components of the angular velocity vector. Given the vector $\omega = [\omega_1,\, \omega_2,\, \omega_3]^T$, the cross map $(\cdot)^\times : \mathbb{R}^3 \to \mathfrak{so}(3)$ is defined as

$$\omega^\times = \begin{bmatrix} 0 & -\omega_3 & \omega_2 \\ \omega_3 & 0 & -\omega_1 \\ -\omega_2 & \omega_1 & 0 \end{bmatrix} \tag{3}$$

The dynamic equations for a rigid body can be expressed in $\mathsf{TSE}(3)$ as

$$\dot{g} = g\mathbb{V}^\vee \tag{4}$$

$$\dot{\mathbb{V}} = \mathbb{I}^{-1}\left(\mathrm{ad}^*_{\mathbb{V}}\mathbb{I}\mathbb{V} + u\right) \tag{5}$$

In (5), the input term u denotes the sum of external inputs u_e and control inputs u_c as shown in (6).

$$u = u_e + u_c \in \mathbb{R}^6 \tag{6}$$

The augmented inertia tensor $\mathbb{I}$ can be defined as

$$\mathbb{I} = \begin{bmatrix} J & 0_{3\times 3} \\ 0_{3\times 3} & mI_3 \end{bmatrix} \in \mathbb{R}^{6\times 6}, \tag{7}$$

such that J is the inertia tensor, $I_3 \in \mathbb{R}^{3\times 3}$ is an identity matrix and the coadjoint operator is defined as

$$\mathrm{ad}^*_{\mathbb{V}} = \mathrm{ad}^T_{\mathbb{V}} = \begin{bmatrix} -\omega^\times & -v^\times \\ 0_{3\times 3} & -\omega^\times \end{bmatrix} \in \mathbb{R}^{6\times 6} \tag{8}$$

where the adjoint operator $\mathrm{ad}_{\mathbb{V}}$ is

$$\mathrm{ad}_{\mathbb{V}} = \begin{bmatrix} \omega^\times & 0_{3\times 3} \\ v^\times & \omega^\times \end{bmatrix} \in \mathbb{R}^{6\times 6} \tag{9}$$

Control Input

The control input u was derived from JWST slew telemetry data. Accordingly, the satellite's attitude control system (ACS) was assumed to be in coarse or fine-guidance mode during this settling time.

$$u = \begin{bmatrix} u_L \\ u_f \end{bmatrix} \in \mathbb{R}^6 \tag{10}$$

The control torque u_L was calculated using commanded torque data from the JWST's ACS. The JWST generates control torques using its six reaction wheel assemblies (RWA). These data were converted from the JWST's geometric J-frame to its body frame for use in $\mathsf{SE}(3)$. This was done by diagonalizing the spacecraft's inertia tensor, provided by [9], using (11) and (12). For an eigenvector $x \in \mathbb{R}^3$, these eigenvalues $\lambda_1, \lambda_2, \lambda_3$ correspond to the principle moments of inertia I_1, I_2, I_3 respectively.

$$\mathbb{I}x = \lambda x \tag{11}$$

$$\mathbb{I}_{diag} = \begin{bmatrix} \lambda_1 & 0 & 0 \\ 0 & \lambda_2 & 0 \\ 0 & 0 & \lambda_3 \end{bmatrix} \tag{12}$$

The control force u_f was assumed to be a zero vector. The JWST typically uses control forces, produced by its propulsion subsystem, to periodically unload angular momentum from its RWAs and to station keep [10]. It can be assumed that neither activity would occur while the spacecraft was settling after a slew.

NUMERICAL SIMULATION

The dynamical model is responsible for calculating the differential states $\dot{g}$ and $\dot{\mathbb{V}}$ using (4) and (5) respectively. Here, the spacecraft's pose g is used to model phenomena such as gravitational attraction f_g, solar radiation pressure (SRP) f_{SRP}, and gravity gradient torque L_{GG}. These terms sum to form the external inputs u_e.

The gravitational force vector f_g acting on a body of mass m due to N other bodies of standard gravitational parameter μ_i, using position vectors r and r_i respectively, is given by

$$f_g = m \sum_{i=1}^{N} \frac{\mu_i (r_i - r)}{\|r_i - r\|^3} \tag{13}$$

The solar radiation pressure f_{SRP} is given by (14). It simplifies the JWST's sun shield to a flat surface, whose orientation with respect to (WRT) to the inertial frame is given by the normal vector $\hat{v}_{ss}$. This paper assumes that this force vector is coincident with the JWST's center of mass, by virtue of the spacecraft's momentum trim flap.

$$f_{SRP} = G_{SC} C_r \cdot \frac{1\text{AU} \cdot A \| r \cdot \hat{v}_{ss} \|}{c \|r\|^3} \cdot \hat{v}_{ss} \tag{14}$$

G_{SC} refers to the solar constant (W/m^2) and C_r refers to the sun shield's coefficient of reflectivity. The orientation $\hat{v}_{ss}$ is given by

$$\hat{v}_{ss} = R_{ss} R \cdot \hat{\imath} \tag{15}$$

where R_{ss} refers to the rotation matrix from the sun-shield normal vector to the body frame. The gravity gradient torque τ_{GG} in the spacecraft body-fixed frame is given in [24] as

$$L_{GG} = \frac{3\mu}{\|r\|^3}(R^T\hat{r})^{\times} J R^T \hat{r} \tag{16}$$

Rigid Body Model

The JWST uses a geometric reference frame, known as the J-frame, affixed to the spacecraft bus. The spacecraft's center of mass lies a few meters away in the +J3 ($z_{\mathcal{G}}$) direction, with the body-fixed frame rotated to match the spacecraft's principle moments of inertia as seen in Fig. 1.

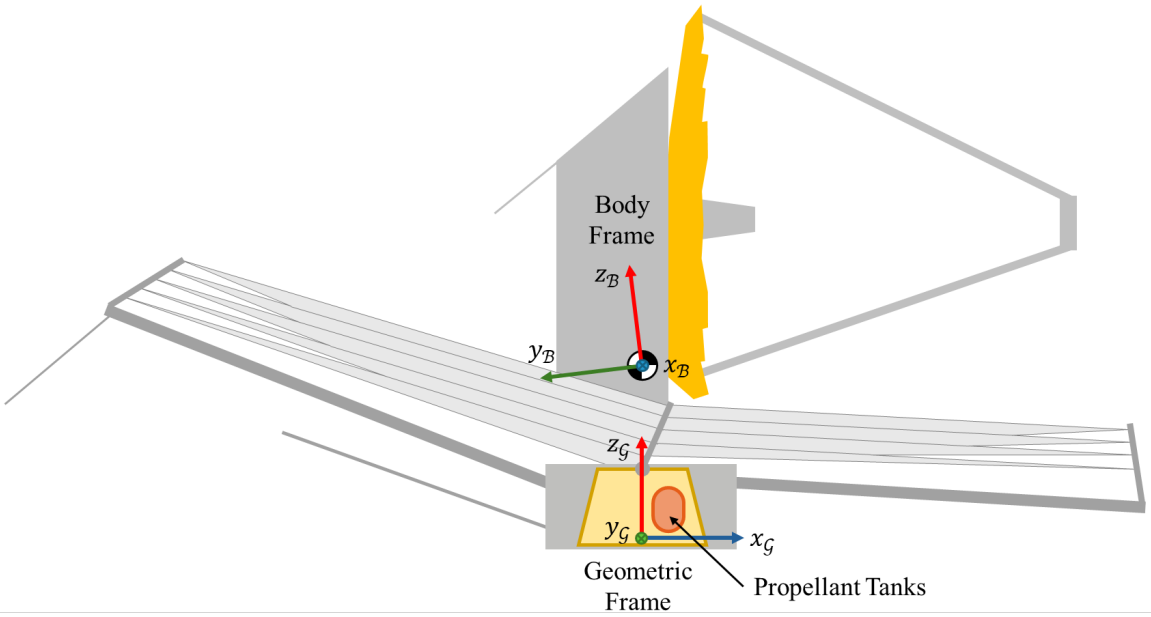

Fig. 1: JWST dimensions and mass breakdown

The distance between the JWST's propellant tanks and its center of mass can couple attitude perturbations to fuel slosh. By simulating the JWST as a rigid body of inertia $\mathbb{I}_{diag}$, this coupling can be isolated via residuals between the true and modeled angular velocities. These residuals would also contain other unmodeled dynamics, such as those caused by the sunshield or by the spacecraft's passive vibration isolators.

N-Body Integrator in $\mathsf{SE}(3)$

A numerical integrator (NI) is responsible for propagating state information forward through time. This paper utilizes the fourth-order Runge-Kutta (RK4) method modified for the $\mathsf{SE}(3)$ framework. The intermediate stage values $k_1, ..., k_4$ are given by (17) through (20).

$$k_1 = f(t_n, y_n) \tag{17}$$

$$k_2 = f(t_n + \frac{h}{2}, y_n + \frac{h}{2}k_1) \tag{18}$$

$$k_3 = f(t_n + \frac{h}{2}, y_n + \frac{h}{2}k_2) \tag{19}$$

$$k_4 = f(t_n + h, y_n + hk_3) \tag{20}$$

A weighted average is then performed in (21) to estimate the next state.

$$y_{n+1} = y_n + \frac{h}{6}(k_1 + 2k_2 + 2k_3 + k_4) \tag{21}$$

The coefficients a_{ij}, weights b_i, and nodes c_i of the RK4 method may be represented by the Butcher tableau in (23).

$$\begin{array}{c|ccc} c_1 & a_{11} & \dots & a_{1s} \\ \vdots & \vdots & \ddots & \vdots \\ c_s & a_{s1} & \dots & a_{ss} \\ \hline & b_1 & \dots & b_s \end{array} \tag{22}$$

$$\begin{array}{c|cccc} \frac{1}{2} & \frac{1}{2} & & & \\ \frac{1}{2} & & \frac{1}{2} & & \\ 1 & & & 1 & \\ \hline & \frac{1}{6} & \frac{1}{3} & \frac{1}{3} & \frac{1}{6} \end{array} \tag{23}$$

By sampling the differential function $f(t, y)$ four times per time step, the RK4 integrator achieves a more accurate propagation than an integrator using the forward Euler method.

Algorithm 1 $\mathsf{SE}(3)$, 4th-Order Runge-Kutta Integrator Logic

Define Initial Conditions $g_1, \mathbb{V}_1$

Begin Main Iteration Loop:

1: **for** $i = 2, ..., 4$ **do**
2: Call Dynamical Model for Stage $i-1$
3: $[\dot{g}_{i-1}, \dot{\mathbb{V}}_{i-1}] = f(g_{i-1}, \mathbb{V}_{i-1})$
4: Propagate Intermediate $\mathbb{V}_i$
5: $\mathbb{V}_i = \mathbb{V}_1 + c_i h \dot{\mathbb{V}}_{i-1}$
6: Propagate Intermediate g_i
7: $\Delta\theta_i = c_i h \omega_i$
8: $R_i = R_1 \cdot \exp(\Delta\theta_i)$
9: $r_i = r_1 + c_i h \dot{r}_{i-1}$
10: $g_i = \begin{bmatrix} R_i & r_i \\ 0_{1\times 3} & 1 \end{bmatrix}$
11: **end for**
12: Call Dynamical Model for Stage 4
13: $[\dot{g}_4, \dot{\mathbb{V}}_4] = f(g_4, \mathbb{V}_4)$
14: Propagate Final $\mathbb{V}$
15: $\mathbb{V} = \mathbb{V}_1 + b_1 h \dot{\mathbb{V}}_1 + b_2 h \dot{\mathbb{V}}_2 + b_3 h \dot{\mathbb{V}}_3 + b_4 h \dot{\mathbb{V}}_4$
16: Propagate Final g
17: $\Delta\theta = h\omega$
18: $R = R_1 \cdot \exp(\Delta\theta_{n+1})$
19: $r = r_1 + b_1 h \dot{r}_1 + b_2 h \dot{r}_2 + b_3 h \dot{r}_3 + b_4 h \dot{r}_4$
20: $g = \begin{bmatrix} R_{n+1} & r_{n+1} \\ 0_{1\times 3} & 1 \end{bmatrix}$ =0

Algorithm 1, which demonstrates the RK4 approximation of g and $\mathbb{V}$ for one time step h, was initially developed in [23]. Past iterations of this $\mathsf{SE}(3)$ RK4 integrator, such as that used in [1], have been limited to propagating the state of only one body. Therefore, an N-body simulation would require for the trajectories of other bodies to be propagated using a more traditional attitude parameterization set. This would also neglect the influence that the spacecraft might impart on the dynamics of these other bodies. For this paper, the NI has been reworked to accept N-bodies through the modification of its matrix operations. An additional dimension was added to most matrices in Algorithm 1 to accommodate N bodies. This requires for the exponential map, seen in stages 8 and 18, to be run in a for-loop once per body.

Simulation Methodology

Initial states for the 11 bodies were generated using ephemeris data from the JPL Horizons system, corresponding to a barycentric dynamical time of A.D. 2023-Aug-10 11:42:44 TDB. These data were generated WRT the J2000.0 epoch international celestial reference frame (ICRF), an inertial barycentric reference frame. This includes ephemeris data for the Sun, the eight innermost planets, the Earth's moon, and the JWST.

The consideration of orbit-attitude coupling for the JWST required the use of a modified algorithm as seen in Fig. 2. After ephemeris data was used to generate an initial state (dashed lines), the spacecraft's attitude (R_k) and angular velocity (ω_k) were updated at every time step using the slew

telemetry data. Although not shown, this also requires for the numerical integrator to rotate position vector r_{k+1} from R_k into the new body frame R_{k+1}.

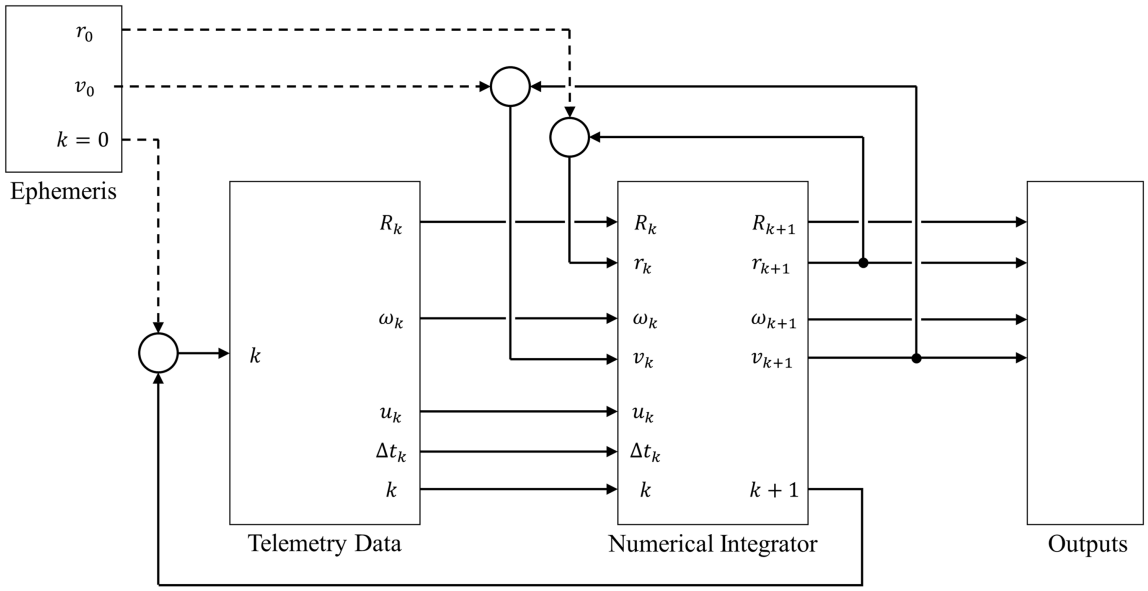

Fig. 2: JWST simulation block diagram

The propagation of position r and linear velocity v is crucial to this methodology, allowing the calculation of telemetry residuals at any given temporal resolution.

RESULTS

The JWST's propagated trajectory is shown in the Sun-Earth rotating reference frame (RRF) in Fig. 3. This propagated halo orbit (solid blue) closely corresponds to the ephemeris data (dashed black).

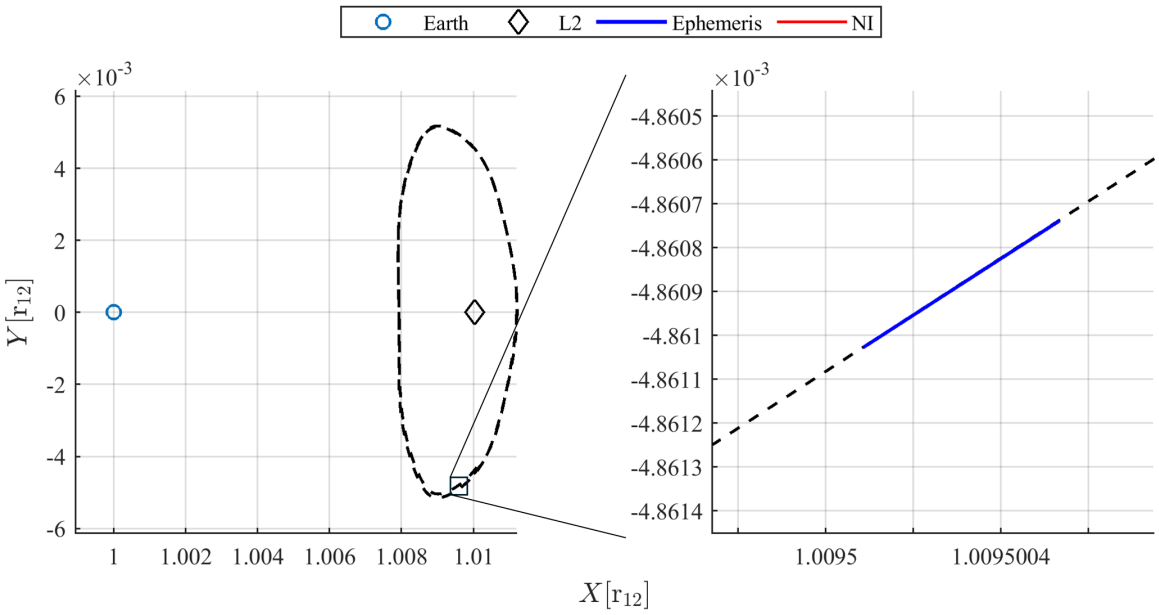

Fig. 3: JWST trajectory propagated by NI, in the Sun-Earth rotating reference frame (RRF).

Fig. 4 displays this JWST positional error as a separation distance between propagated and ephemeris trajectories WRT the ICRF. This error grows exponentially to a maximum of 4.796 m after approximately 600 s. This error was predominantly in the normal direction to the ecliptic plane.

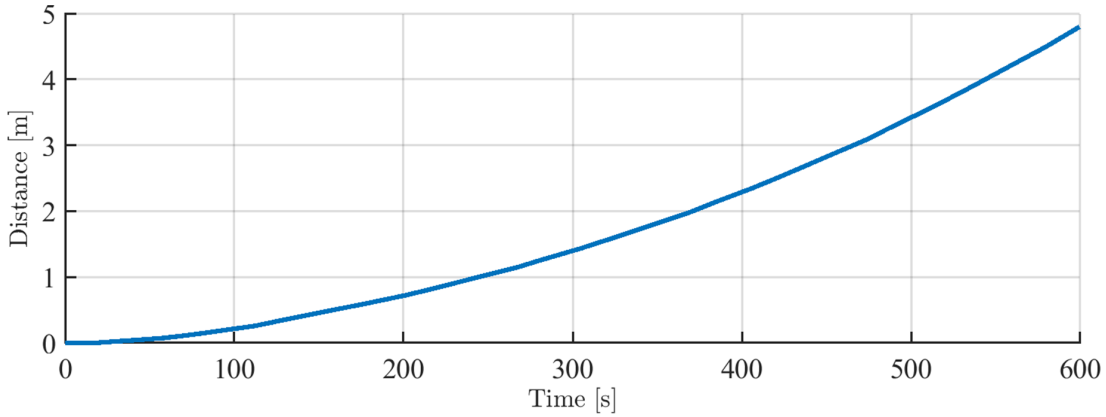

Fig. 4: Trajectory error of the JWST NI vs. JWST ephemeris.

The slew telemetry data shown in Fig. 5-7 corresponds to the settling time after a coarse slew maneuver conducted on A.D. 2023-Aug-10 11:42:44.2380 UTC. Fig. 5 shows the body torque commanded by the spacecraft's attitude control subsystem (ACS). This commanded torque notably

features large oscillations on the order of 0.01 Hz. The matching data for all three J-frame axes suggests an error in the slew telemetry data generation.

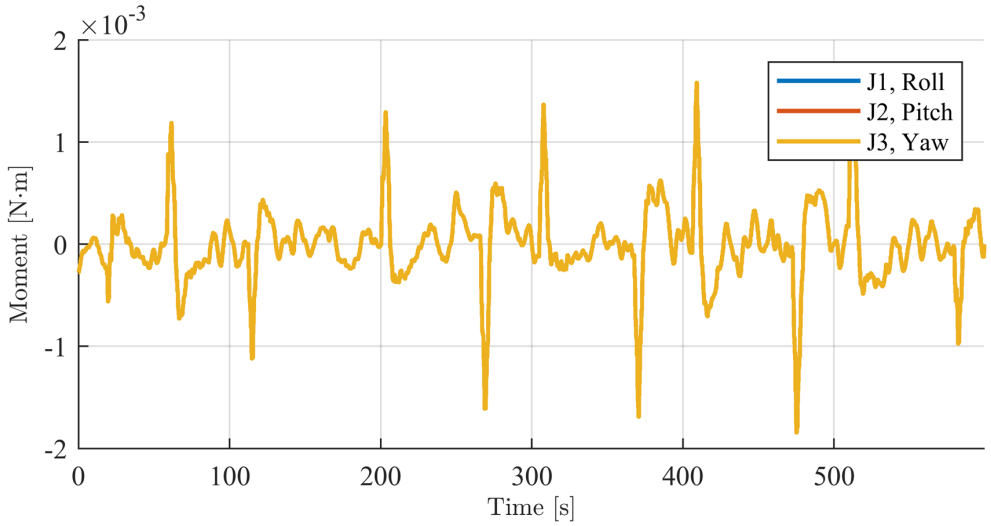

Fig. 5: JWST ACS commanded body torque, in the geometric frame.

Fig. 6 presents the modeled, true, and residual angular velocities for the JWST. Commanded torque was seen to have negligible effect on the residual angular velocities until made several orders of magnitude greater.

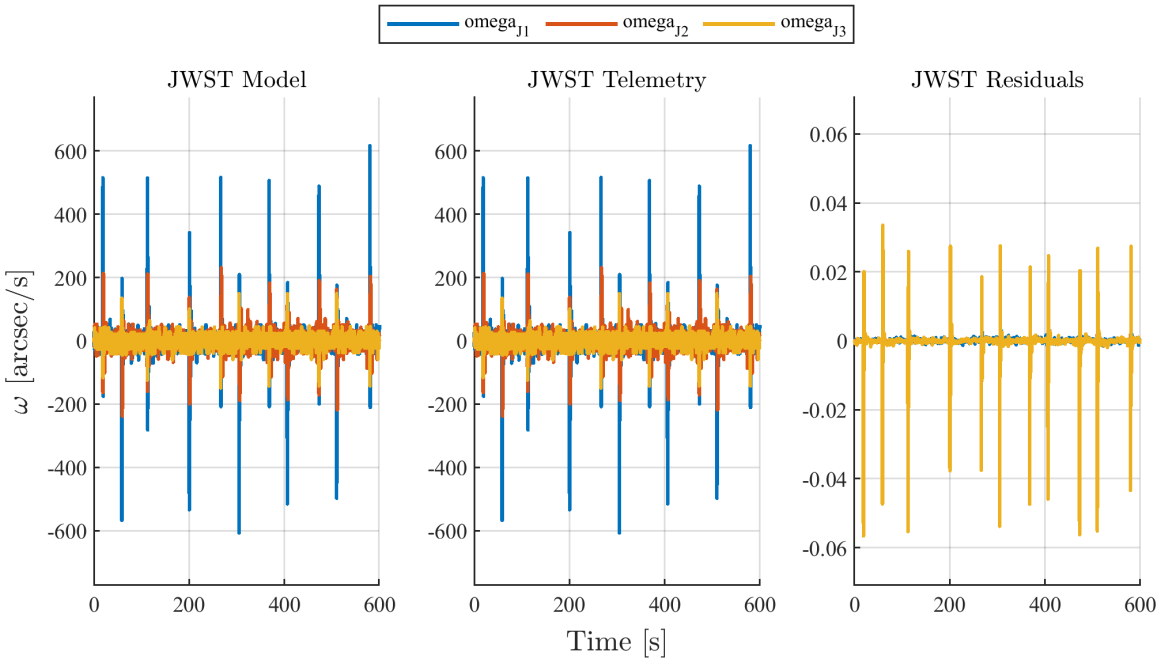

Fig. 6: JWST angular velocity from model, slew telemetry data, and model residuals.

A frequency analysis was performed on the true and residual angular velocity data using a fast Fourier transform (FFT). These data require further analysis, but [27] names several JWST vibra-

tional modes below 1 Hz in frequency.

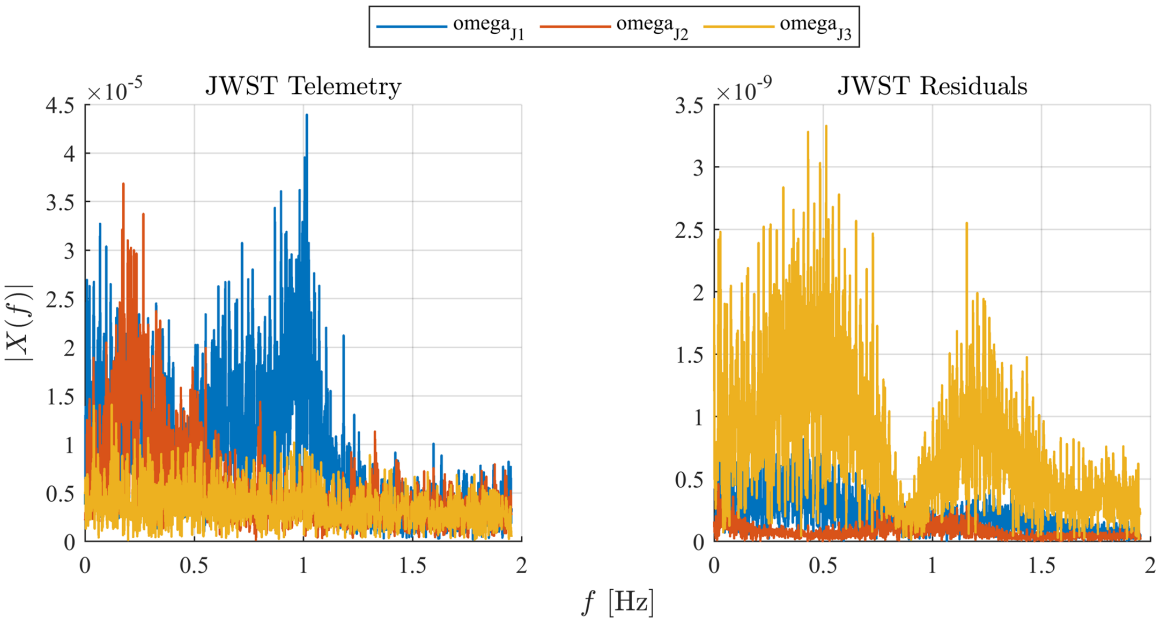

Fig. 7: JWST angular velocity Fourier transform for slew telemetry data and model residuals.

CONCLUSIONS AND FUTURE WORK

An N-body integrator has been developed for the problem of fuel slosh estimation for the James Webb Space Telescope. This NI references a dynamical model to simulate the motion of the JWST in 6-DoF to allow for the comparison of its attitude perturbations with recorded slew telemetry data. This work may enable enhanced methods of simulating nonlinear systems and extracting nonlinear motion from noisy data.

The frequency analysis performed on the JWST's angular velocity residuals suggests that the unmodeled dynamics preferentially affect certain frequencies for each of the J-frame axes. The analysis of both the true and residual angular velocities did not reveal any notable behavior near 0.045 Hz, a fuel slosh frequency identified by [27] via line-of-sight jitter analysis. Although higher frequency slosh modes may still be present, this suggests that this method may not be suitable for the purpose of fuel slosh analysis.

Nevertheless, an N-body $\mathsf{SE}(3)$ integrator–as developed in this paper–may still be well-suited for simulating the rendezvous, proximity operations, and docking (RPOD) of bodies whose masses are within a few orders of magnitude of one another.

ACKNOWLEDGMENTS

The authors would like to acknowledge Dr. Morad Nazari for his development of a numerical integrator in special Euclidean group $\mathsf{SE}(3)$, from which much of this work has been inspired.

REFERENCES

[1] M. M. Wittal, B. W. Asher, and M. Nazari, "Autonomous RPOD For Arbitrarily Configured Spacecraft with Anomaly Detection," *AAS/AIAA Astrodynamics Specialist Conference*, 2024.

[2] M. A. Clark, A. Pensado, C. A. Jones, M. L. Grande, and E. Judd, "How the Allocation of Lander Functions Impacts Human Lunar Exploration Architecture Propellant Demands," *AIAA SciTech Forum*, 2021, https://doi.org/10.2514/6.2021-0627.

[3] Y. Yan and B. Yue, "Stability analysis of liquid filled spacecraft system with flexible attachment by using the energy–Casimir method," *Theoretical and Applied Mechanics Letters*, Vol. 6, No. 2, 2016, pp. 100–106, https://doi.org/10.1016/j.taml.2016.03.001.

[4] H. N. Abramson, "The Dynamic Behavior of Liquids in Moving Containers," Technical Report NASA SP-106, Southwest Research Institute, 1967.

[5] J. M. Storey, D. Kirk, H. Gutierrez, B. Marsell, and P. A. Schallhorn, "Experimental, Numerical and Analytical Characterization of Slosh Dynamics Applied to In-Space Propellant Storage, Management and Transfer," *51st AIAA/SAE/ASEE Joint Propulsion Conference*, 2015, https://doi.org/10.2514/6.2015-4077.

[6] M. Fagetti, B. McCann, M. Nazari, M. Wittal, and J. Smith, "Mass and Inertia Property Estimation on TSE(3) in the Presence of a Sloshing Liquid," *AAS/AIAA Space Flight Mechanics Meeting*, 2023.

[7] W. J. Elke III, J. Pei, C. M. Roithmayr, and R. J. Caverly, "Framework for Analyzing the Complex Interactions Between Spacecraft Motion and Slosh Dynamics in Low-G Environments," *International Astronautical Congress*, 2022, https://doi.org/10.13140/RG.2.2.33205.35041.

[8] C. Dennehy and O. S. Alvarez-Salazar, "Spacecraft Micro-Vibration: A Survey of Problems, Experiences, Potential Solutions, and Some Lessons Learned," Technical Memorandum NASA/TM2018-220075, National Aeronautics and Space Administration, 2018.

[9] L. Meza, F. C. Tung, S. M. Anandakrishnan, V. A. Spector, and T. T. Hyde, "Line of Sight Stabilization of James Webb Space Telescope," *27th Annual AAS Guidance and Control Conference*, 2005.

[10] M. Menzel, M. Davis, K. Parrish, J. Lawrence, A. Stewart, J. Cooper, S. Irish, G. Mosier, M. Levine, J. Pitman, G. Walsh, P. Maghami, S. Thomson, E. Wooldridge, R. Boucarut, L. Feinberg, G. Turner, P. Kalia, and C. Bowers, "The Design, Verification, and Performance of the James Webb Space Telescope," *Publications of the Astronomical Society of the Pacific*, Vol. 135, 2023, https://doi.org/10.1088/1538-3873/acbb9f.

[11] D. J. Dichmann, C. M. Alberding, and W. H. Yu, "Stationkeeping Monte Carlo Simulation for the James Webb Space Telescope," *International Symposium on Space Flight Dynamics 2014*, 2014.

[12] F. T. Dodge, "The New "Dynamic Behavior of Liquids in Moving Containers"," technical report, Southwest Research Institute, 2000.

[13] F. Saltari, A. Traini, F. Gambioli, and F. Mastroddi, "A linearized reduced-order model approach for sloshing to be used for aerospace design," *Aerospace Science and Technology*, Vol. 108, 2011, https://doi.org/10.1016/j.ast.2020.106369.

[14] W. Tam and D. Jaekle, "Design and Qualification of Fuel and Oxidizer Tank Assemblies for the James Webb Space Telescope," *Space Propulsion 2018*, 2018.

[15] W. W. Benson, N. Dennehy, B. Marsell, T. VanZwieten, and J. Orr, "Low-G Slosh Workshop Results From 2023: State of the Art, Gaps and Forward Work," *46th Annual AAS Guidance, Navigation and Control (GNC) Conference*, 2024.

[16] J. M. Storey, D. Kirk, B. Marsell, and P. Schallhorn, "Progress towards a Microgravity CFD Validation Study using the ISS SPHERES-SLOSH Experiment," *AIAA/SAE/ASEE Joint Propulsion Conference*, 2017, https://doi.org/10.2514/6.2020-3814.

[17] M. M. Wittal, W. Dziedzic, J. S. Pitt, B. McCann, M. Fagetti, and M. Nazari, "Modeling Low-G Slosh Using Negative Mass," *46th Rocky Mountain AAS GNC Conference*, 2024.

[18] B. Pridgen, K. Bai, and W. E. Singhose, "Shaping Container Motion for Multimode and Robust Slosh Suppression," *Journal of Spacecraft and Rockets*, Vol. 50, No. 2, 2013, pp. 440–448, https://doi.org/10.2514/1.A32137.

[19] Q. Hu, "Input shaping and variable structure control for simultaneous precision positioning and vibration reduction of flexible spacecraft with saturation compensatio," *Journal of Sound and Vibration*, Vol. 318, No. 1, 2008, pp. 18–35, https://doi.org/10.1016/j.jsv.2008.03.068.

[20] T. D. Tuttle and W. P. Seering, "Vibration Reduction in Flexible Space Structures Using Input Shaping on MACE: Mission Results," *IFAC Proceedings Volumes*, Vol. 29, No. 1, 1996, pp. 1500–1505, https://doi.org/10.1016/S1474-6670(17)57879-9.

[21] W. Singhose, "Command shaping for flexible systems: A review of the first 50 years," *International Journal of Precision Engineering and Manufacturing*, Vol. 10, No. 4, 2009, pp. 153–168, https://doi.org/10.1007/s12541-009-0084-2.

[22] T. Lee, M. Leok, and N. H. McClamroch, "Lie Group Variational Integrators for the Full Body Problem," *Computational Methods in Applied Mechanics and Engineering*, Vol. 196, No. 8, 2005, https://doi.org/10.1016/j.cma.2007.01.017.

[23] D. Seo and M. Nazari, "Rigid Body Adaptive Stabilization on the Tangent Bundle of the LIE Groups," *AIAA SciTech Forum*, 2019, https://doi.org/10.2514/6.2019-0653.

[24] G. Mangiacapra, M. Wittal, E. Capello, and M. Nazari, "Unscented Kalman Filter and Control on TSE(3) with Application to Spacecraft Dynamics," *Nonlinear Dynamics*, Vol. 108, No. 3, 2022, pp. 2127–2146, https://doi.org/10.1007/s11071-022-07293-x.

[25] B. McCann, M. Nazari, and C. Petersen, "Numerical Approaches for Constrained and Unconstrained, Static Optimization on the Special Euclidean Group SE(3)," *Journal of Optimization Theory and Applications*, Vol. 201, No. 3, 2024, pp. 1116–1150, https://doi.org/10.1007/s10957-024-02431-4.

[26] J. Sola, J. Deray, and D. Atchuthan, "A micro Lie theory for state estimation in robotics," *2018 arXiv preprint*, 2018, arXiv: 1812.01537.

[27] J. Rigby, M. Perrin, M. McElwain, R. Kimble, S. Friedman, M. Lallo, R. Doyon, L. Feinberg, P. Ferruit, A. Glasse, M. Rieke, G. Rieke, G. Wright, C. Willott, K. Colon, S. Milam, S. Neff, C. Stark, J. Valenti, J. Abell, F. Abney, Y. Abul-Huda, D. S. Acton, E. Adams, D. Adler, J. Aguilar, N. Ahmed, L. Albert, S. Alberts, D. Aldridge, M. Allen, M. Altenburg, J. Álvarez-Márquez, C. Alves de Oliveira, G. Andersen, H. Anderson, S. Anderson, I. Argyriou, A. Armstrong, S. Arribas, E. Artigau, A. Arvai, C. Atkinson, G. Bacon, T. Bair, K. Banks, J. Barrientes, B. Barringer, P. Bartosik, W. Bast, P. Baudoz, T. Beatty, K. Bechtold, T. Beck, E. Bergeron, M. Bergkoetter, R. Bhatawdekar, S. Birkmann, R. Blazek, C. Blome, A. Boccaletti, T. Böker, J. Boia, N. Bonaventura, N. Bond, K. Bosley, R. Boucarut, M. Bourque, J. Bouwman, G. Bower, C. Bowers, M. Boyer, L. Bradley, G. Brady, H. Braun, D. Breda, P. Bresnahan, S. Bright, C. Britt, A. Bromenschenkel, B. Brooks, K. Brooks, B. Brown, M. Brown, P. Brown, A. Bunker, M. Burger, H. Bushouse, S. Cale, A. Cameron, P. Cameron, A. Canipe, J. Caplinger, F. Caputo, M. Cara, L. Carey, S. Carniani, M. Carrasquilla, M. Carruthers, M. Case, R. Catherine, D. Chance, G. Chapman, S. Charlot, B. Charlow, P. Chayer, B. Chen, B. Cherinka, S. Chichester, Z. Chilton, T. Chonis, M. Clampin, C. Clark, K. Clark, D. Coe, B. Coleman, B. Comber, T. Comeau, D. Connolly, J. Cooper, R. Cooper, E. Coppock, M. Correnti, C. Cossou, A. Coulais, L. Coyle, M. Cracraft, M. Curti, S. Cuturic, K. Davis, M. Davis, B. Dean, A. DeLisa, W. deMeester, N. Dencheva, N. Dencheva, J. DePasquale, J. Deschenes, Ö. Hunor Detre, R. Diaz, D. Dicken, A. DiFelice, M. Dillman, W. Dixon, J. Doggett, T. Donaldson, R. Douglas, K. DuPrie, J. Dupuis, J. Durning, N. Easmin, W. Eck, C. Edeani, E. Egami, R. Ehrenwinkler, J. Eisenhamer, M. Eisenhower, M. Elie, J. Elliott, K. Elliott, T. Ellis, M. Engesser, N. Espinoza, O. Etienne, M. Etxaluze, P. Falini, M. Feeney, M. Ferry, J. Filippazzo, B. Fincham, M. Fix, N. Flagey, M. Florian, J. Flynn, E. Fontanella, T. Ford, P. Forshay, O. Fox, D. Franz, H. Fu, A. Fullerton, S. Galkin, A. Galyer, M. García Marín, J. P. Gardner, L. Gardner, D. Garland, B. Garrett, D. Gasman, A. Gaspar, D. Gaudreau, P. Gauthier, V. Geers, P. Geithner, M. Gennaro, G. Giardino, J. Girard, M. Giuliano, K. Glassmire, and A. Glauser, "Characterization of JWST science performance from commissioning," *Publications of the Astronomical Society of the Pacific*, Vol. 135, No. 1046, 2023, https://doi.org/10.48550/arXiv.2207.05632.